Transformation of metallic photonic structures from nano-hole to nano-island arrays through annealing process

Hongmei Liu (刘红梅)[1], Zhaoguang Pang (庞兆广)[1,2], Tianrui Zhai (翟天瑞)[1], and Xinping Zhang (张新平)[1*]

[1] *College of Applied Sciences, Beijing University of Technology, Beijing 100124, China*

[2] *College of Physics Science and Information Engineering, Hebei Normal University, Shijiazhuang 050024, China*

[*] *Corresponding author: zhangxinping@bjut.edu.cn*

Received December 30, 2011; accepted February 20, 2012; posted online June 20, 2012

Large-area metallic photonic crystals (MPCs) consist of two-dimensional (2D) periodical arrays of gold nano-holes are fabricated by solution-processible gold nanoparticles using interference lithography in combination with subsequent lift-off and annealing processes. By controlling the annealing temperature, the 2D nano-hole arrays are transformed into nano-island arrays, enabling easy achievements of two different photonic devices. The microscopic characterization shows convincingly the success of the fabrication techniques and verifies our proposed mechanisms for this kind of nanoscale morphology transformation. This kind of mechanisms can be applied extensively in the metallic nanofabrication and in the realization of plasmonic photonic devices.

OCIS codes: 250.0250, 100.6640, 210.4770, 180.1790.

doi: 10.3788/COL201210.S12502.

Metallic photonic crystals (MPCs) are spatially periodical arranged nano-structures of the noble metals. Such structures have attracted increasing attention because of their unique optoelectronic properties playing a remarkable role in current nanoscience, where their special optical properties can be applied to optical polarziers[1], optical filters[2], all-optical switching[3], distributed–feedback lasers[4], and biosensors[5−7]. Different methods have been demonstrated for fabrication of the MPCs, including those based on electron beam lithography (EBL)[8,9], nano-imprinting lithography (NIL)[10−12], and focused ion beam (FIB) lithography[13−15]. However, these methods are expensive, and can only prepare small-area (several to hundreds micrometers) samples, which brings great inconvenience for application of the MPCs to devices. Solution-processible method enables simple, low-cost, large scale, and mass fabrication of the gold subwavelength structures[16,17]. In this letter, we report a solution-processible method to fabricate the two-dimensional (2D) MPCs consist of nano-hole arrays, and then we transform the 2D nano-hole arrays into nano-island arrays just by controlling the annealing temperature. The microscopic characterization shows the 2D nano-hole arrays and nano-island arrays are well arranged. Particle plasmon resonance (PPR) of the 2D MPCs and its coupling with the resonance mode of the planar waveguide excited by underneath the nano-hole or nano-particle arrays has also been characterized. In both the TM and TE incident polarizations, the 2D nano-island arrays show strong coupling between the plasmon resonance and waveguide mode in the spectrum rang from 560 to 650 nm when tuning the incident angle from 0° to 20°.

The fabrication procedure of the 2D nano-hole arrays is illustrated in Fig. 1. Firstly, the nanocylinder grating mask was fabricated using interference lithography. Secondly, gold colloid with the concentration of 100 mg/ml was spin-coated onto the surface of the 2D grating-mask at a speed of 2 000 rpm for 30 min. Afterwards the sample was heated at 150 °C for 5 min to decompose the

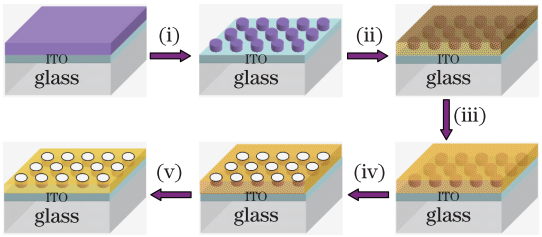

Fig. 1. Process for fabricating the 2D nano-hole arrays: (i) preparation of the photoresist mask-grating using interference lithography; (ii) spin-coating of gold colloid solution onto the photoresist mask-grating; (iii) annealing at 150 °C for 5 min; (iv) rinsing with acetone to lift off the photoresist; (v) annealing at 250 °C for 20 s.

ligands modified around the gold nanoparticles. After the sample was cooled down to the room temperature, it was rinsed with acetone to lift off the photoresisit. At last, making use of the low melting temperature of the gold nanoparticles[18,19], the samples were annealed at 250 °C on a hot plate for 20 s to melt the gold nanoparticles and form the gold nano-hole arrays. When the samples (before or after the photoresist was lifted off) were heated at 450 °C in a furnace for 10 min, the 2D nano-hole arrays were transformed into nano-island arrays. The process from nano-hole arrays to forming nano-island arrays is estimated in Fig. 2. Firstly, the gold film around the nano-holes with the thickness of 40–50 nm melted at 450 °C and shrinked because of the large surface tension of the molten gold, result in diameter expanding of the nano-holes arrays; and then the gold film broke into pieces at the thinnest place between two adjacent nano-holes; at last, with the help of the large surface tension of the molten gold, the gold pieces further shrinked and formed the well arranged gold nano-island arrays. The thickness of the ITO waveguide is 200 nm deposited on a 1-mm-thick glass substrate. The synthesis of the gold nanoparticles for preparing the colloidal gold nanoparticles is detailed in Refs. [20], and the mean size

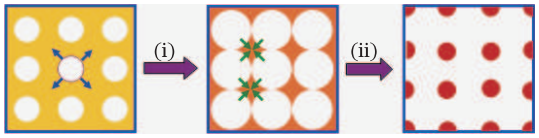

Fig. 2. Mechanism of nano-hole arrays transforming into nano-island arrays with the annealing temperature increasing to 450 °C; (i) diameter expanding of the nano-holes arrays; (ii) shrinking of the gold film to form the gold nano-island arrays.

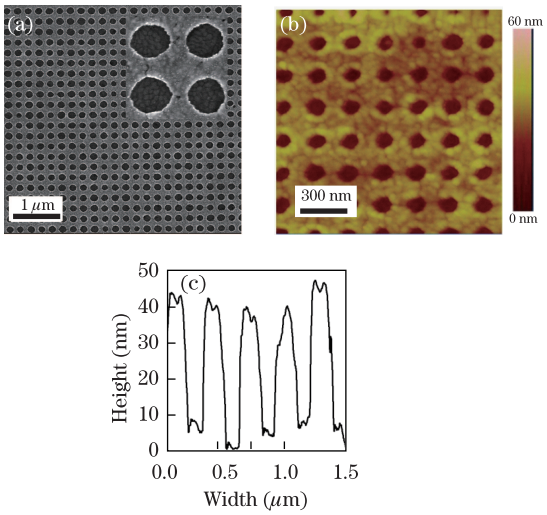

Fig. 3. (a) SEM and (b) AFM images of the 2D metallic nano-holes arrays fabricated using a mask grating of nano-cylinders with a diameter of about 150 nm and a depth of 50 nm; (c) cross-section of the 2D nano-hole arrays. Inset of (a): HR-SEM image of the nano-holes.

is about 1.5–5 nm in diameter. The positive photoresist (S1 805, Rohm and Haas Electronic Materials Ltd.) has been used as received. The 325-nm He-Cd laser was used as the UV source for interference lithography to fabricate the photoresist nano-gratings.

Figures 3(a)–(c) shows the high resolution scanning-electron-microscopy (HR-SEM) and the atomic force microscopy (AFM) images of the 2D nano-hole photonic crystal structures. When the 2D nano-holes arrays are fabricated on a flat waveguide, such as 200 nm ITO, the waveguide coupled 2D nano-hole arrays are obtained. From the HR-SEM image we found that the gold film around the holes was continuous and the photoresist was completely lifted off from the substrate because we can observe the grains of the ITO surface from the inset of Fig. 3. The period of the nano-hole arrays are about 330 nm with a mean diameter about 200 nm. AFM image in Fig. 3(b) shows the film around the nano-holes is smooth with a roughness less than 5 nm. From the cross-section of the AFM image shown in Fig. 3(c) we found that the mean depth of the nano-holes was about 45 nm, according to the distance between two adjacent nano-holes, we could calculate the aspect ratio of the area bearing PPR in the visible wavelength as 2.2. Figure 4 shows the HR-SEM and AFM images of the 2D nano-island arrays, it can be found from the SEM image that the gold nano-islands are well arranged except for a little disturbance, which convinces that the shrinking process brings small disturbance to the nano-island arrays. The period of the nano-island arrays is around 330 nm. From the cross section of the AFM image in Fig. 4(c) we found that the gold nano-islands had a mean height about 90 nm and a mean diameter of about 150 nm. So the aspect ratio of the gold nano-islands can be calculated as 0.8.

Optical properties of the nano-hole arrays fabricated on the ITO glass substrate are characterized, in Fig. 5. PPR can be observed in the spectrum from 500 to 900 nm with the intensity of about 0.4 OD and the full width at half maximum (FWHM) of about 200 nm. The peak is centered at 700 nm. The angle-resolved tuning properties of the waveguided 2D periodical nano-hole MPC are shown in Figs. 5(a) and (b). For TM polarization, due to the broad band PPR spectum excited in nano-hole arrays, coupling can be observed in the wavelength from 650 to 750 nm with increasing the incident angle from 32° to 64°. The coupling is relatively weak, because the poor overlapping of the PPR of the nano-hole arrays and the waveguide mode. Similar optical properties can also be obtained for TE polarization in Fig. 5(b) which demonstrates the uniformity of the nano-hole arrays in the two directions.

The angle-resolved tuning properties of the waveguided 2D periodical nano-islands are shown in Figs. 6(a)

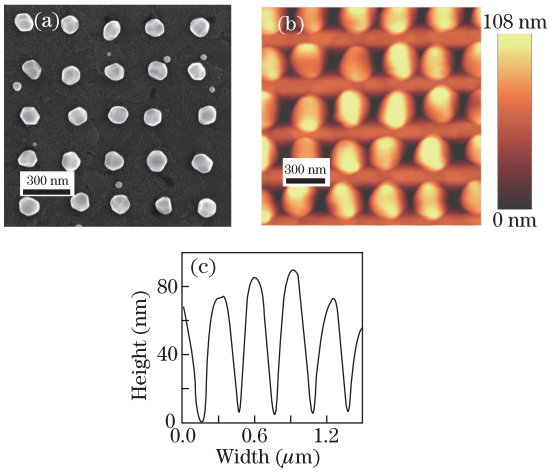

Fig. 4. (a) SEM and (b) AFM images of the 2D nano-island arrays fabricated using a mask grating of nanocylinders with a diameter of about 150 nm and a depth of 50 nm; (c) cross-section of the 2D nano-island arrays.

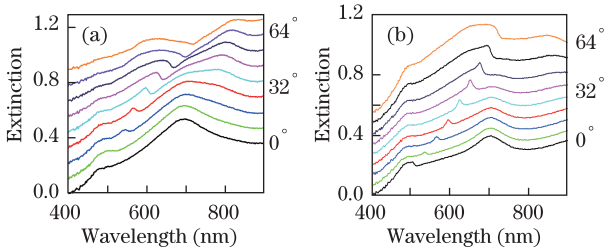

Fig. 5. Optical extinction spectra of the 2D nano-hole arrays for (a) TM and (b) TE polarizations, respectively, with the incident angle θ varying from 0° to 56° in steps of 8°.

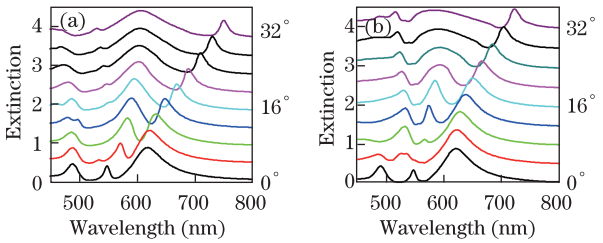

Fig. 6. Optical extinction spectra of the 2D nano-island arrays fabricated on the ITO substrates for different incident polarization for (a) TM and for (b) TE polarizations, respectively, with the incident angle θ varying from 0° to 32° in steps of 4°.

and (b). We found that when the nano-hole arrays was transformed to nano-island arrays at high annealing temperature, the FWHM of the PPR of the gold nano-islands was decreased to 50 nm and blue-shifted to 606 nm with a very high extinction amplitude of 0.9 OD. The exciting wavelength of the plasmon resonant is determined by the aspect ratios and the surrounding refractive index of the gold nano-structures, so that the great difference of the extinction spectra between the nano-hole arrays and the nano-island arrays is mainly because of their different aspect ratios. Large aspect ratio brings to narrow and blue-shifting of the PPR for the nano-island arrays and small aspect ratio at the area between two adjacent nano-holes brings to broad and red-shifting of the spectrum. At normal incidence, coupling between the waveguide mode and the PPR of the gold nano-islands arrays can be observed in Fig. 6(a) at 560 nm for TM polarization. With the increasing of the incident angle from 0° to 20°, strong coupling between the PPR and the waveguide mode in the longer-wavelength branch can be observed in the spectrum rang from 560 to 650 nm. As the incident angle is increased over 20°, the waveguide mode is gradually tuned out of the spectral range of the PPR, and shows the extinction peaks in the spectra. Similar properties can also be obtained for TE polarization in Fig. 6(b) which demonstrates the uniformity of the nano-hole arrays in two directions.

In conclusion, we demonstrate fabrication of MPC structures consisting of gold nanohole arrays using the solution processible technique with the lift-off procedure included, and successful transformation of the nano-hole into the nano-island MPCs through changing the annealing temperatures. The spectroscopic properties give distinct comparison between the optical responses of these two kinds of MPCs. This fabrication technique provides flexible approaches for the realization of plasmonic photonic structures.

This work was supported by the National Natural Science Foundation of China (Nos. 11074018 and 11104007), the Program for New Century Excellent Talents in University, the Research Fund for the Doctoral Program of Higher Education of China (No. 20091103110012), the Beijing Educational Commission (No. KM201210005034), and the Natural Science Foundation of Hebei Province (No. A2012205085).

References

1. X. P. Zhang, H. M. Liu, J. R. Tian, Y. R. Song, J. Y. Song, and L. Wang, Nano Lett. **8,** 2653 (2008).
2. X. P. Zhang, H. M. Liu, J. R. Tian, Y. R. Song, L. Wang, J. Y. Song, and G. Z. Zhang, Nanotechnol. **19,** 285202 (2008).
3. X. P. Zhang, B. Q. Sun, J. M. Hodgkiss, and R. H. Friend, Adv. Mater. **20,** 4455 (2008).
4. E. B. Namdas, M. H. Tong, P. Ledochowitsch, S. R. Mednick, J. D. Yuen, D. Moses, and A. J. Heeger, Adv. Mater. **20,** 1 (2008).
5. J. K. Prashant, W. Huang, and A. E. Mostafa, Nano Lett. **7,** 2080, (2007).
6. X. Zhang, F. Dou, and H. Liu, Nanotechnol. **21,** 335501 (2010).
7. X. Zhang X. Ma, F. Dou, P. Zhao, and H. Liu, Adv. Funct. Mater. **21,** 4219 (2011).
8. J. K. Prashant, W. Huang, and A. E. Mostafa, Nano Lett. **7,** 2080 (2007).
9. C. L. Haynes, A. D. McFarland, L. L. Zhao, R. P. Van Duyne, and G. C. Schatz, J. Phys. Chem. B **107,** 7337 (2003).
10. H. L. Chen, S. Y. Chuang, H. C. Cheng, C. H. Lin, and T. C. Chu, Microelectron. Eng. **83,** 893 (2006).
11. G. Zhang, J. Zhang, G. Xie, Z. Liu, and H. Shao, Small **2,** 1440 (2006).
12. B. D. Lucas, J. S. Kim, C. Chin, and L. J. Guo, Adv. Mater. **20,** 1129 (2008).
13. S. Cabrini, A. Carpentiero, R. Kumar, L. Businaro, P. Candeloro, M. Prasciolu, A. Gosparini, C. Andreani, M. DeVittorio, T. Stomeo, and E. DiFabrizio, Microelectron. Eng. **11,** 78 (2005).
14. S. Reyntjens and R. J. Puers, Micromech. Microeng. **10,** 181 (2000).
15. M. Ishida, J. Fujita, T. Ichihashi, Y. Ochiai, T. Kaito, and S. J. Matsui, Vac. Sci. Technol. B **21,** 2728 (2003).
16. X. P. Zhang, B. Q. Sun, R. H. Friend, H. C. Guo, D. Nau, and H. Giessen, Nano Lett. **6,** 651 (2006).
17. X. P. Zhang, B. Q. Sun, R. H. Friend, H. C. Guo, N. Tetreault, H. Giessen, and R. H. Friend, Appl. Phys. Letts. **90,** 133114 (2007).
18. P. Buffat and J. P. Borel, Phys. ReV. A **13,** 2287 (1976).
19. D. Huang, F. Liao, S. Molesa, D. Redinger, and V.Subramanian, J. Electrochem. Soc. **150,** G412 (2003).
20. M. J. Hostetler, J. E. Wingate, C. J. Zhong, J. E. Harris, R. W. Vachet, M. R. Clark, J. D. Londono, S. J. Green, J. J. Stokes, G. D. Wignall, G. L. Glish, M. D. Porter, N. D. Evans, and R. W. Murray, Langmuir **14,** 17 (1998).